5.1

Systematic Differences of Rainfall Estimates in TRMM 3G68

T. Nakazawa and K. Rajendran*

*CSSPR/JST, Meteorological Research Institute, Tsukuba, Japan.

1. Introduction

The successful operation of the Tropical Rainfall Measuring Mission (TRMM) satellite since its launch in November 1997, provided continuous rainfall data for more than 7-years and enabled the scientific community to use it as a base data set for many application studies. One of the primary objectives of the TRMM was to measure the tropical/subtropical rainfall rate with maximum accuracy. However, recent studies (Kummerow et al. 2000; Berg et al. 2002) have shown that significant difference between rainfall estimates from the precipitation radar(PR) and the TRMM Microwave radiometer instrument(TMI) exists even after applying several revisions to the algorithms for these two onboard sensors of TRMM, which are independently measuring the same system. Kummerow et al. (2000) have shown that there is a quarter of order difference between the rain estimates from the two algorithms with PR underestimating rain compared to TMI.

There have been many studies using TRMM data, explaining the possible sources of differences between TMI and PR estimates (e.g., Berg et al. 2002; Masunaga et al. 2005). In addition, recent studies(Kim et al. 2004; Nesbitt et al. 2004) suggest the importance of melting layer effect on TMI rain estimation. Kim et al. (2004) found that inclusion of melting layer effect can reduce TMI rain estimates especially over ocean. Nesbitt et al. (2004) speculated that the TMI overestimation with respect to PR is related not only with ice-scattering signatures in 85 GHz, but also due to the non-inclusion of melting-layer emission in Version 5 of the TMI algorithm. Our main focus in this study is to understand the characteristics of the systematic rainfall differences between TMI and PR utilizing the gridded ASCII product of TRMM and address the possible reasons in terms of large-scale features which can lead to these differences in rainfall estimates over the tropics.

2. Data

TRMM 3G68 version 5 dataset provides, unconditional rain rates (Runco), total pixel number (Ntot), rain pixel number (Nrain), and percentage of convective rain (Pconv) over 0.5°× 0.5°based on the standard products of PR 2A25 (radar algorithm, Iguchi et al. 2000), TMI 2A12 (passive microwave algorithm, Kummerow et al. 2001) and 2B31 (combined algorithm, Haddad et al. 1997) from 1997 to present. Using these four quantities, we derived additional two quantities such as conditional rain rate (Rcond) and rain cover percentage (Pcover) which are also used for the present analysis. By assuming the sum of rain over a sensor swath within a 0.5° × 0.5°box as Sum(R), we can derive Rcond and Runco from the following relationship:

Sum(R) = Runco × Ntot = Rcond × Nrain

Hence, Rcond is obtained as Sum(R)/Nrain. The rain cover percentage,Pcover, is calculated as,

Pcover = Nrain / Ntot × 100.

For the present analysis we have utilized these datasets for the period 1998-2003. The daily values are computed from the hourly gridded ASCII data sets obtained from http://trmmopen.gsfc.nasa.gov. Since our main objective is to identify the distinct and systematic differences between these products, we constructed a 'masked' dataset of TMI taking into account the difference between its swath area with PR swath and also to coincide with the observational area. Thus, the masked data of TMI is constructed on the PR swath by ignoring the data points within TMI swath on which PR data were not available.

In addition, we have analyzed the 3G01 gridded Visible Infrared Scanner (VIRS) infrared (Channel 4) mean brightness temperature products representing the cloud top height of a given storm.

3. Results

Figure 1 shows the relationship between TMI and PR conditional rain rates over the equatorial Pacific during February 1998 as a function of their respective convective percentages. The circle symbols indicate the differences where the PR rain estimates are larger than TMI and the triangle symbols indicate the differences where the TMI rain estimates are larger compared to PR. In this figure we excluded the points with the values of the differences (TMI-PR) between -1 and 1 mm/hr. The percentage of this range falls for rainfall difference greater (smaller) than (-1) mm/hr is

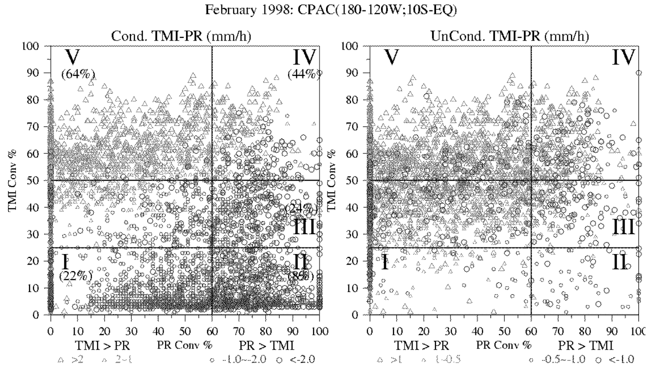

Fig. 1: Rcond rain differences between TMI and PR data over equatorial Central Pacific (180° - 120° W; 10° S - EQ) during February 1998 as a function of their respective convective percentages representing different phases of the life cycle of organized convection.

23% (37%) and 44% (35%) for conditional and unconditional rain respectively. The horizontal and vertical solid lines and the markers 'I' to 'VI' are for delineating and representing different convective regimes, which is discussed in detail in the later part of this section. Comparison between TMI and PR conditional rain rate with their respective convective percentages shows that PR overestimates rainfall compared to TMI when Pconv(TMI) is smaller than Pconv(PR) (lower right side in each panel of Fig. 1) and TMI overestimate rainfall when Pconv(TMI) is larger than PR (upper left side in respective panels).

We have observed similar features over different oceanic domains and also for different time period of observation. This is found to be a general feature for most of the equatorial oceans with less sensitivity to the ENSO-related changes in convective activity. However, our analysis is restricted to equatorial oceanic domains because of the unavailability of convective percentage estimates from TMI over the land points in version 5 data sets.

Figure 2 shows the distribution of TMI and PR rain cover percentages as a function of TMI and PR convective percentages. Pcover is computed as the percentile value of the ratio between the number of rainy pixels and the total number of pixels within each half degree bin as described above. It can be seen that Pcover(TMI) also exhibits largest rain cover values when Pconv(TMI) is greater than 25% and Pconv(PR)is less than 60%. In addition, Pcover(TMI) shows an increasing tendency with Pconv(TMI) similar to TMI rain rates. Pcover(PR) also exhibit similar tendency as of Pcover(TMI) with convective percentages.

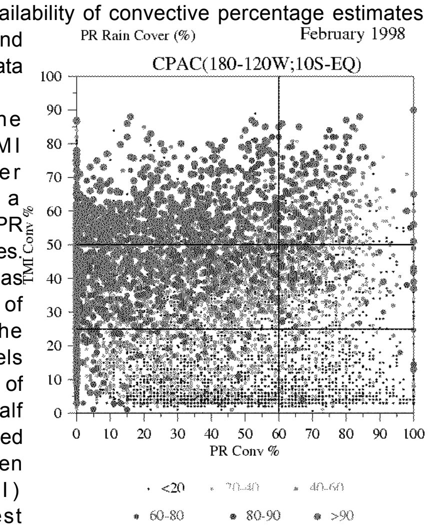

Fig. 2: Pcover (TMI) over Central Pacific during February 1998 are plotted as a function of PR and TMI convective percentages.

To further understand the relation between the variation of convective percentage with cloud informations such as brightness temperature, we have analyzed gridded VIRS Channel 4 brightness temperature data from the same satellite. Here, we have treated brightness temperature as a proxy for the cloud top height. Figure

3 shows the mean brightness temperature over Central Pacific during February 1998 as a function of PR and TMI convective percentages. If both PR and TMI estimates are close, the minimum brightness temperature should cluster towards the higher convective percentages. However, it is observed that the low brightness temperature values are more skewed towards lower Pconv(PR) and with Pconv(TMI) above 30 %.

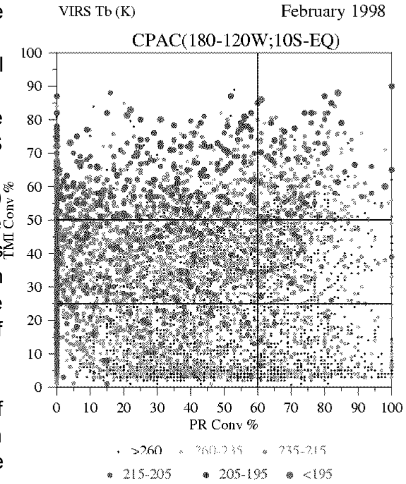

Fig. 3: VIRS Channel 4 mean brightness temperature over Central Pacific during February 1998 are plotted as a function of PR and TMI convective percentages.

By analysing the rainfall differences (Fig. 1), rain cover percentage (Fig. 2) and the VIRS Channel 4 mean temperature (Fig. 3) as a function of the convective percentages of PR and TMI, we can identify and delineate distinct life stages of convective storms.

We have identified six different stages of convection based on Figures 1 to 3 and these different convective regimes are delineated with solid lines in respective figures. We suggest that there exists a coherent relationship between the rain estimate differences and the different stages of the life cycle of convection (e.g., in Fig. 1, regimes I to V). For example, it can be seen from Fig. 1 that TMI rain estimates are larger than PR when the Pconv(TMI) is high and Pconv(PR) is low, Pcover is high and cloud top is high (denoted as regime 'V') and PR rain is larger than TMI in lower-right when Pconv(TMI) is low and Pconv(PR) is high, Pcover is small (< 20%) and cloud top is low (Tb is warmer than 260° K, denoted as regime 'II'). In regimes I and II, during the formative stage of the convection, the TMI algorithm is not able to capture the rain accurately (where PR estimates are found to be larger). This tendency still exists during the developing phase of convection (regime III, which can be inferred from region where the respective convective percentages are about 30%-50%, as seen in Fig. 2). During the mature phase in regime IV, both the estimates match closely. The markedly large TMI overestimation occurs at high Pconv(TMI) (> 50%) and low Pconv(PR) (regime V) which implies the dissipation stage and subsequent later phase of decaying stage of convection [regime VI with moderate Pconv(TMI) and low Pconv(PR)].

The relative percentage of pixels with mean brightness temperature below 240° K which can be considered as a proxy for deep convection is computed for each regime over the two ocean domains. It reveals that the maximum number of low brightness temperature pixels are located for regimes V and VI. This clearly indicates that over the ocean, highest cloud tops occurs during regimes V and VI where TMI yields highly overestimated rain estimates. Hence, during mature to dissipation stage (regime V and VI), the differences in TMI and PR rain estimates arise not only due to melting layer effect of stratiform anvil type remnants of the dissipating clouds (Nesbitt et al. 2004) but also from the ice-scattering effect of the overshooting tops of deep clouds and resultant increased back-radiation from the ice particles. When PR observes this cloud, the rain intensity is not comparable to that from TMI, because in many cases there is no root of rain in the anvil cloud. This is further supported with the high rain cover percentage (Fig. 2) and low brightness temperature maximum over this regime (Fig. 3).

4. Conclusions

In this study the systematic differences between rainfall estimates from TMI and PR datasets of TRMM-3G68 version 5 are analyzed and possible reason for the differences between them are addressed. TRMM TMI rainfall estimates are found to be larger than PR estimates over most of the equatorial tropics. The distribution of conditional rainfall differences between TMI and PR with respect to their respective convective percentages revealed coherent relationship between these rain differences with different convective/ stratiform regimes. We speculate that these distinct differences are associated with different life stages of organised convection. The Rcond(PR) estimates are found to be larger compared to TMI when Pconv(PR) and Pconv(TMI) are low which can be associated with formative stages of convection. This suggests that during the formative stages of convection, PR rain algorithm estimates relatively more conditional rain than TMI. When Pconv(TMI) is low and Pconv(PR) is high, can be treated as initial phase of developing convection, PR rain estimates are found to be still larger over most of the equatorial oceans. But when TMI and PR convective percentages are above 60% which can be considered as the later phase of the developing stage of convection, both the estimates are found to be comparable.

Further, it is shown that large discrepancy between the two data sets occurs during the mature to decay phases of convection, with TMI considerably overestimating the rain rates. One plausible reason for this significantly large difference can be due to the lag between the time of maximum rain rate and the time of maximum cloud top height (the time of maximum cloud top height lags the time of maximum rain rate). PR may capture the right timing of the maximum surface rain rate. If we compare the TMI rain rate with PR at this time, the difference is not large. This corresponds to regime IV. However, the cloud top height for cumulonimbus may raise further and solid water particles develops in the upper troposphere with less rainfall below, which may result that the TMI rain rate having a maximum at this time (regime V or VI). Consequently, during the mature to dissipating phase of convection, due to the existence of overshooting tops of tall clouds comprising anvil type of remnants with melting layer, TMI is likely to overestimate rain through both large ice-scattering effect near the cloud top and the lack of melting layer emission effect in the Version 5 TMI algorithm. This is further analyzed utilizing the cloud informations from the Visible Infrared Scanner (VIRS) brightness temperature of the same satellite. During these phases, the variation of brightness temperature correspondingly reflects higher cloud top heights and also suggests the possibility of TMI overestimation and its links to ice-scattering and melting layer effects. Further evaluation of major conclusion of the present analysis in the context of Version 6 product is left for the future analysis.

Acknowledgments

The help of Dr. S. Sajani, VSSC, India, during the initial stages of the analysis are gratefully acknowledged.

References

Berg, W., C. D. Kummerow, and C. A. Morales, 2002: Differences between East and West Pacific rainfall systems. J. Climate, 15, 3659–3672.

Haddad, Z. S., E. A. Smith, C. D. Kummerow, T. Iguchi, M. R. Farrar, S.L. Durden, M. Alves, and W. S. Olson, 1997: The TRMM 'Day-1'Radar/ Radiometer Combined Rain-Profiling Algorithm. J. Meteor.Soc. Japan, 75, 799–809.

Iguchi, T., T. Kozu, R. Meneghini, J, Awaka, and K. Okamoto, 2000: Rain-profiling algorithm for the TRMM precipitation radar. J. Appl. Meteor., 39, 2038–2052.

Kim, M.-J., J. A. Weinman, and R. A. Houze, 2004: Validation of maritime rainfall retrievals from the TRMM microwave radiometer. J. Appl. Meteorol., 43, 847–859.

Kummerow, C. D., and Co-authors, 2000: The status of the Tropical Rainfall Measuring Mission (TRMM) after two years in orbit. J. Appl. Meteorol., 39, 1965–1982.

Kummerow, C. D., and Co-authors, 2001: The evolution of the Goddard profiling algorithm (GPROF) for rainfall estimation from passive microwave sensors. J. Appl. Meteorol., 40, 1801–1820.

Masunaga, H., T. S. L'Ecuyer, and C. D. Kummerow, 2005: Variability in the characteristics of precipitation systems in the Tropical Pacific. Part I: Spatial Structure. J. Climate, 18, 823–840.

Nesbitt, S. W., E. J. Zipser, and C. D. Kummerow, 2004: An examination of version-5 rainfall estimates from the TRMM microwave imager, precipitation radar, and rain gauges on global, regional, and storm scales. J. Appl. Meteorol., 43, 1016–1036.

Short, D. A., and K. Nakamura, 2000: TRMM radar observations of shallow precipitation over the tropical oceans. J. Climate, 13, 4107–4124.